ASME Journal of Electrochemical Energy Conversion and Storage
Online journal at:
https://asmedigitalcollection.asme.org/electrochemical

Critical Role of Mixing for Dry Processing Sodium Ion Cathodes

Ruihao Deng
Department of Mechanical, Aerospace and Nuclear Engineering,
Rensselaer Polytechnic Institute,
Troy, NY 12180
e-mail: dengr2@rpi.edu

Ruixin Wu
Department of Mechanical, Aerospace and Nuclear Engineering,
Rensselaer Polytechnic Institute,
Troy, NY 12180
e-mail: wur11@rpi.edu

Fudong Han[1]
Department of Mechanical, Aerospace and Nuclear Engineering,
Rensselaer Polytechnic Institute,
Troy, NY 12180
e-mail: hanf2@rpi.edu

Due to the elimination of solvent removal and recovery, dry electrode processing has enabled significant reductions in energy consumption and cost for lithium-ion battery (LIB) manufacturing. However, transferring this promising manufacturing approach to sodium-ion batteries (SIBs), of which cost is the primary driver for technological development, has been surprisingly rare, with clear knowledge gaps in understanding the process–structure–performance relationship. Here, we investigate the effects of each step (mixing, calendaring, and laminating) during dry processing of an O3-type $NaNi_{0.33}Fe_{0.33}Mn_{0.33}O_2$ (NFM) cathode on the microstructure and electrochemical performance. We highlight the critical role of appropriate mixing for fabricating a high-performance dry-processed electrode. Insufficient mixing may lead to nonuniform distribution of the polytetrafluoroethylene (PTFE) in the electrode composite, which, upon laminating, can migrate to the electrode surface, leading to poor wetting between the liquid electrolyte and the cathode, while excessive mixing can lead to surface degradation of the cathode active materials due to the reduction of Ni. As the wetting ability of liquid electrolyte on the electrode is not a serious concern for LIBs, our work provides novel insights that are specific to sodium cathodes for the development of scalable, low-cost, sustainable dry processes for SIB manufacturing. [DOI: 10.1115/1.4070290]

Keywords: sodium-ion cathodes, dry processing, manufacturing, batteries, electrochemical engineering, electrochemical storage, innovative material synthesis and manufacturing methods, novel materials, reliability, durability and damage tolerance

Introduction

Lithium-ion batteries (LIBs) have enjoyed their success in powering portable electronics and are considered the most promising technology for electric vehicles and grid storage. Full-scale development of LIBs in these applications poses significant challenges in the manufacturing of this technology in terms of both financial and environmental impacts [1–5]. The predominant method for battery manufacturing is based on the slurry casting process. The process consists of mixing active material, polymer binder, and conductive additive in a solvent, typically N-methyl-pyrrolidone (NMP), slurry casting, drying, and calendaring to form electrode sheets. Owing to its high toxicity, NMP needs to be recycled [1,4]. Despite being verified as an industrially scalable process, the coating, drying, and recovery steps consume a significant amount of energy (46% of the total energy for battery manufacturing) and make up about 17% of the total manufacturing cost [5,6]. The slurry casting process also faces challenges in fabricating thick cathodes due to binder migration during the drying stage, leading to uneven distribution of electrode components and even electrode cracking [7].

Thereby, there is a growing interest in developing solvent-free or dry processes for electrode manufacturing [8–14]. Particularly, the dry process based on polytetrafluoroethylene (PTFE) fibrillation, initially developed by Maxwell Technologies and later acquired by Tesla, has attracted significant interest [11,15]. The process involves a dry mixing treatment for PTFE fibrillation together with active material and conductive additive, calendaring/rolling the resultant powder mixture into a free-standing electrode film, and laminating the free-standing electrode onto a current collector [11]. The dry processing approach not only reduces the environmental footprint by eliminating toxic solvent emissions but also significantly simplifies the fabrication process, reduces energy consumption, and lowers the manufacturing cost. The fibrillation of PTFE forms a network to support active material and conductive carbon, which helps maintain the uniform distribution of the electrode component during fabrication, especially for thick electrodes, leading to improved electrochemical performance [16]. Significant research has been done to employ the approach to fabricate LIB electrodes including $LiCoO_2$ [17], $LiFePO_4$ (LFP) [18–20], $LiNi_xMn_yCo_zO_2$ $(x+y+z=1)$ [21–23], $LiNi_xCo_yAl_zO_2$ $(x+y+z=1)$ [24], $LiMn_2O_4$ [25], and $LiNi_{0.5}Mn_{1.5}O_4$ [26] cathodes, and carbon [9,27], silicon [28], and $Li_4Ti_5O_{12}$ [29] anodes. However, the electrochemical stability of PTFE with low-voltage anodes still needs to be improved.

The success of the dry processing of LIB electrodes has led to the development of the technology for fabricating electrodes and electrolytes for emerging battery technologies such as solid-state batteries [8,30–34] and lithium-sulfur batteries [35], and the approach has demonstrated great success in reducing

[1]Corresponding author.

Manuscript received August 16, 2025; final manuscript received October 30, 2025; published online November 12, 2025. Assoc. Editor: Ömer Özgür Çapraz.

manufacturing costs and improving electrochemical performance. Nevertheless, the application of dry processing for manufacturing sodium-ion batteries (SIBs), of which low cost is a major driver for technological development, has been surprisingly rare [14]. SIBs are considered an important alternative for LIBs primarily due to the increased abundance and availability of sodium [36,37]. Additional cost savings are related to the replacement of the copper anode current collector with aluminum. Nevertheless, due to the relatively low energy density of SIBs, it is under intense debate within the battery community whether SIBs can be economically competitive, in terms of dollars per kW h, when compared with low-cost LIBs based on LFP cathode, at least in the near term [38,39]. The cost of SIBs is mainly determined by the cost of raw materials and manufacturing costs. Significant efforts are being devoted to developing advanced electrode and electrolyte materials with a lower cost and a higher energy density [40]. However, reducing the manufacturing costs of SIBs, which may play a key role in improving the competitiveness of the technology, has been largely overlooked by the community. In this regard, the development of low-cost dry process technology for SIB manufacturing may help pave the way for its large-scale deployment. In addition, as many sodium layered oxides seem to be more sensitive to moisture than their lithium counterparts [41], dry processing of the SIB electrode may also improve its electrochemical performance due to the elimination of a long solvent drying process which may lead to moisture contamination. Moreover, the specific capacities of typical sodium-ion cathodes (<140 mA h/g) are less than the state-of-the-art nickel-rich lithium layered oxides (~200 mA h/g), and therefore to achieve a similar areal capacity of lithium cathodes (4–6 mA h/cm^2), sodium cathodes will have to be made much thicker, where dry processing can be quite advantageous.

Despite these great promises, reports on dry processing SIB electrodes are very limited. Qin et al. utilized a dry processing approach to fabricate a $Na_3V(PO_4)_3$ cathode for studying the presodiation of the cathode using $Na_2C_2O_4$ [42]. Kühn et al. reported a dry-processed P2-type $Na_{0.75}Ni_{0.25}Fe_{0.25}Mn_{0.50}O_2$ cathode, which exhibited a comparable specific capacity and cycling stability to the solution-processed cathodes [43]. Most recently, Wu et al. studied the effect of particle size of $NaCrO_2$ on the microstructure and electrochemical performance of the dry-processed cathodes and demonstrated that the utilization of larger microsized particles helps to improve mechanical strength and electrochemical performance [44]. These reports provide first-hand information on the feasibility of using dry processing for SIB manufacturing. However, the studied cathodes all face serious challenges for practical applications due to the low volumetric energy density of the $Na_3V(PO_4)_3$ cathode, the low initial coulombic efficiency of a P2-type cathode when paired with a hard carbon anode due to Na insufficiency, and the inclusion of scarce and expensive metals in $NaCrO_2$, respectively [40]. More importantly, none of the reports studied the effect of processing (mixing, calendaring, and laminating) on the microstructure and electrochemical performance of the electrodes. The integration and linking of these subprocesses during dry electrode manufacturing have yet to be revealed [14]. Knowledge gaps remain in understanding the processing–structure–performance relationship of an industrially relevant Na cathode to develop optimal dry processes for SIB manufacturing.

Herein, we report the first comprehensive study on understanding the effect of each step (mixing, calendaring, and laminating) on dry processing O3-type $NaNi_{0.33}Fe_{0.33}Mn_{0.33}O_2$ (NFM) cathodes. NFM is considered one of the most promising cathodes for high-energy-density SIBs because of its high capacity, high Na content, and relatively low content of Ni [39]. Combining processing development, materials characterization, and electrochemical testing, we highlight the critical role of dry mixing for dry processing of Na layered oxide cathode and report fundamental insights that are specific to Na layered oxide cathodes for the development of scalable, low-cost dry processing technology for SIB manufacturing.

Experimental Section

Dry Processing of Electrodes. To fabricate the dry-processed cathode film, commercial active material ($NaNi_{1/3}Fe_{1/3}Mn_{1/3}O_2$ (NFM) from MTI Corporation, USA), conductive carbon black (TIMICAL SUPER C45), and PTFE binder (Teflon^{TM} PTFE 601 X, Fluorogistx) with a specific weight ratio were premixed in a mortar for 10 min. The mixture was then ball-milled in a 50 mL stainless-steel jar with ten 10 mm-diameter grinding balls at 100 rpm for 1, 3, 5, and 10 h. The ball-milled mixture was then manually rolled on the vertical hot platform at 60 °C until all the powders were bonded together and then transferred to the electric hot rolling press (MTI Corporation) with a rolling gap of 100 μm. The free-standing film was then laminated onto the current collector at a temperature of 100 °C with 80 μm for the gap and 1 mm/s for rolling speed.

Material Characterizations. The morphology of the surfaces of ball-milled powders and the cross-section of laminated electrodes were obtained by a Zeiss Supra 55 scanning electron microscope (SEM). The surface chemistry of ball-milled powders was tested by PHI VersaProbe II X-ray photoelectron spectroscopy (XPS). The spatial resolution of this technique is about 10 mm, with a spectral resolution of <0.1 eV, and the XPS signal is obtained from regions within about 5 nm of the surface. The crystal structure and composition of ball-milled powder and laminated film were provided by Panalytical Empytrean X-ray diffraction (XRD). The system runs with a three-axis cradle as a reflection layout (with a motorized sample stage that enables sample tilts, in-plane rotation, and vertical Z displacement). High-resolution goniometer with optically encoded sample positioning enables a minimum step size of 0.001 deg.

Cell Fabrication and Electrochemical Measurement. CR2032 coin cells featured fresh sodium metal foil as the counter electrode and Whatman Grade GF/C glass microfiber. The electrolyte was prepared by dissolving $NaClO_4$ (1.0 M) in a mixed solvent of fluorinated ethylene carbonate (FEC) and propylene carbonate (PC) in a volume ratio of 3:97. All coin cells were assembled in an argon-filled glove box, and the O_2 and H_2O content were both below 0.1 ppm. All electrodes were punched into round discs with a diameter of 10 mm by a precision disc cutter (MTI Corporation, USA), followed by 10 h drying in a vacuum oven at 80 °C. The resulting NFM electrodes exhibit areal loadings of about 2 mA h/cm^2 and active material mass loadings of about 16 mg/cm^2. The electrochemical performances of the electrodes were tested using an Arbin BT 2000 battery cycler.

Results and Discussion

Figure 1 shows the schematic of dry processing NFM cathodes. The XRD peaks of the NFM can be attributed to an O3-type layered oxide, and the NFM exhibits a pellet-like morphology with a particle size of around 5–10 μm (Supplemental Figure 1 available in the Supplemental Materials on the ASME Digital Collection). NFM cathode active material, carbon black, and PTFE binder with a specific weight ratio were first mixed by a planetary ball mill at 100 rpm for different durations. The weight ratio of carbon black is fixed at 3%, while the weight ratio of PTFE changes from 1% to 3% to study the effect of binder content. The content of NFM active material in the studied electrode is greater than 94%, consistent with industrial electrode formulations [39]. The milling duration was increased from 1 h to 10 h to study the effect of dry mixing. The mixed powders were rolled and calendared into a free-standing film, which was then laminated on a current collector to form the final electrode sheet.

To understand the effect of dry mixing, we first performed structure and morphology analysis of the composite powder after mixing for various durations. No impurity phase can be observed

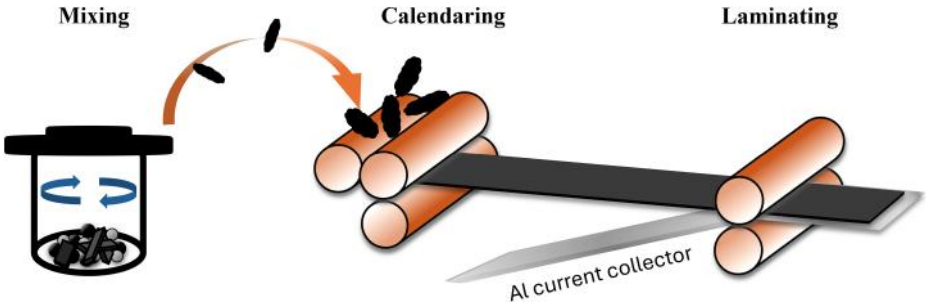

Fig. 1 Schematic of dry processing NFM cathodes

for all the cathode composites (Fig. 2(*a*)), indicating that the mild milling at 100 rpm cannot change the bulk structure of the cathode, although a preferred orientation toward (003) can be observed for 5-h mixing and 10-h mixing cathode composites, probably caused by the orientation of pellet-like particles due to shear during milling. While there is no apparent change in the particle size of the NFM particle (Fig. 2(*b*)), the electrode components became increasingly uniform with the increase of the milling durations, as reflected from the elemental mapping of the composite powders (Fig. 2(*b*)).

The cathode composite powders were then rolled/calendared to form a free-standing film. A large-area film (5 cm × 7.5 cm) could be fabricated for cathode composites with various PTFE contents and milled for various durations (Supplemental Figure 2). The free-standing films obtained after calendaring had a typical thickness of about 100 μm, a density of about 1.7 g/cm^3, and a porosity of about 30%. The porosity of the calendared cathode is consistent with typical dry-processed cathodes [22,44]. The results suggest the excellent film-forming capability of the cathode even at a low content of PTFE (1 wt%). We then tried to laminate the free-standing film onto various current collectors, including stainless-steel mesh, bare Al foil, and etched Al foil. This step has been proven challenging for dry-processed electrodes [14] because the adhesion between the free-standing electrode film and the current collector is primarily based on mechanical interlocking rather than chemical bonding. While we were able to successfully laminate the film onto a stainless-steel mesh (Supplemental Figure 3), which has been commonly used in the literature for evaluating the electrochemical performance of dry-processed cathodes, this step cannot be applied to practical SIBs due to the use of heavy stainless-steel current collectors. However, laminating the free-standing film onto bare Al current collectors has proven difficult. Several delaminations can be observed for the electrode with 1% PTFE, and wrinkles and cracks can be observed for the cathode with 2% and 3% PTFE (Fig. 3(*a*)). On the other hand, the utilization of an etched Al foil with a submicron surface roughness allows good adhesion between the cathode film and the current collector, even at a small content of PTFE (Fig. 3(*b*)). Supplemental Figure 4 shows pictures of the laminated electrodes with various PTFE contents and mixing durations. The great adhesion between the cathode and the current collector was also demonstrated by the cross-sectional SEM images (Fig. 3(*c*)), where no apparent interface can be observed between the etched Al foil and the cathode.

The electrochemical performance of the laminated NFM cathodes was then tested in half-cells with Na metal as the reference and counter electrode and 1 M $NaClO_4$ in a mixed solvent of PC and FEC with a volume fraction of 97:3. It should be noted that while PC has usually been excluded as the solvent for LIBs because of its nonpassivating behavior on the graphite anode, it is a very popular solvent for SIBs that allows high solubility of typical Na salts for a higher ionic conductivity and enables the formation of good solid electrolyte interphase (SEI) on Na metal or

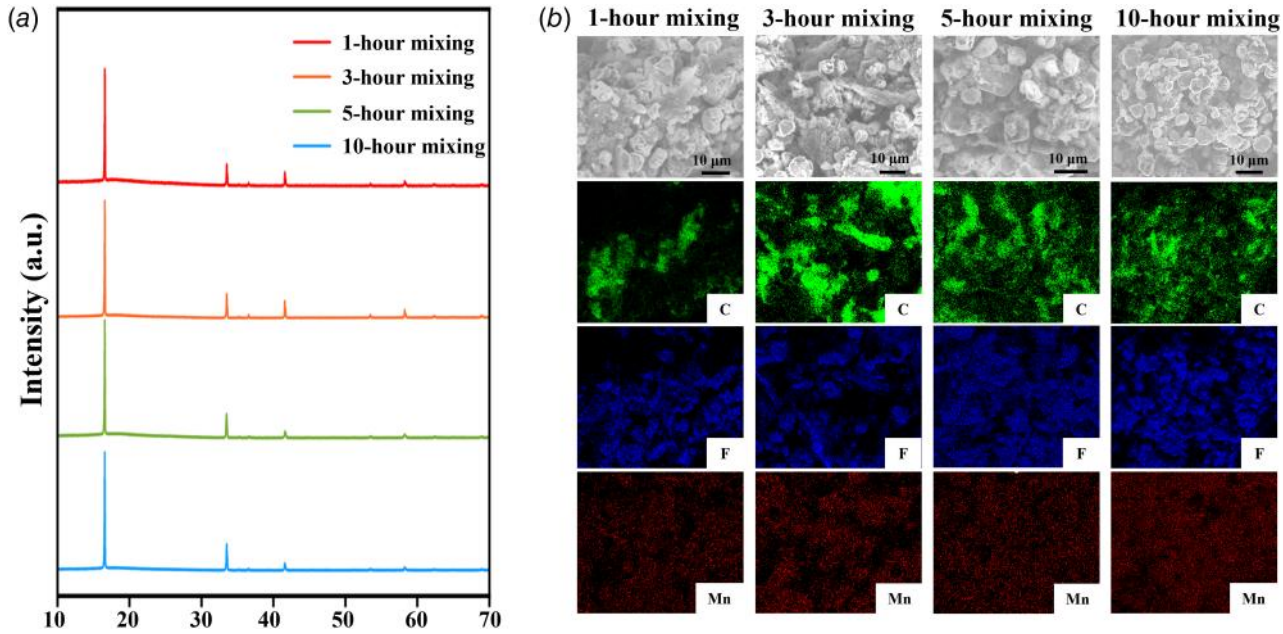

Fig. 2 X-ray diffraction (*a*) and SEM and elemental mappings (*b*) of NFM/PTFE/carbon composite powders mixed with varying durations

hard carbon anode [40]. Figure 4 shows the charge/discharge curves of the dry-processed NFM electrode. The PTFE content decreases from 3% to 1% from left to right, and the mixing duration increases from 1 h to 10 h from top to bottom. While all cathodes with various PTFE contents and mixing durations can be successfully laminated on an etched Al current collector, they exhibit drastically different electrochemical performance. The first observation is that the electrochemical performance is strongly related to the mixing duration and not much to the binder content (Fig. 4). Surprisingly, the first charge of 1-h mixing cathodes cannot be completed, and the results were confirmed for more than five repeated tests. All three cathodes with various PTFE contents exhibit a long charging voltage profile at around 3.0–3.6 V versus Na/Na^+ (Figs. 4(*a*)–4(*c*)). The 3-h mixing cathodes exhibit typical voltage profiles for charge/discharge of NFM cathodes (Figs. 4(*d*)–4(*f*)). As the mixing duration increased to 5 h, the cathodes demonstrated a higher specific capacity with a lower overpotential, and a clearer voltage plateau can be observed (Figs. 4(*g*)–4(*i*)). Further increasing the mixing duration to 10 h led to significant performance degradation. A sharp decrease in the specific capacity and an increase in the overpotential can be observed (Figs. 4(*j*)–4(*l*)). Minimal changes can be observed for cathodes with the same mixing duration but different binder contents, especially for 10-h mixing cathodes (Figs. 4(*j*)–4(*l*)) where electrochemical performance decreases as the PTFE content decreases. The results highlight the critical role of mixing conditions in the electrochemical performance of dry-processed NFM cathodes.

The results from the impedance analysis are consistent with the observations from the voltage profile. Figure 5(*a*) shows the fitting of the Nyquist plots of dry-processed NFM cathodes after various mixing durations. We attributed the high-frequency semicircle to the SEI, and the low-frequency semicircle to charge transfer resistance [45]. R_{SEI} and R_{CT} values are also summarized in Supplemental Table 1. R_{SEI} remained relatively low for the 3-h mixing (7.538 Ω) and 5-h mixing (8.121 Ω) electrodes but increased to 31.1 Ω for the 10-h mixing electrodes. The charge transfer resistance first decreased from 182.3 Ω to 118.7 Ω when the mixing duration increased from 3 h to 5 h, and then sharply increased to 348.3 Ω as the mixing duration increased to 10 h. The semicircles observed from the Nyquist plots (Fig. 5(*a*)) correspond to the interfacial resistance of the dry-processed NFM cathodes in a Na metal half-cell [45]. The interfacial resistance first decreases and then increases as the mixing duration increases from 3 h to 10 h. Moreover, a similar trend can also be observed for the cycling stability (Fig. 5(*b*)) tested at 1C. Rate capability testing (Supplemental Figure 5) further demonstrates that, within the range of 0.05–5C, the 5-h mixed electrode consistently delivers a higher reversible capacity than the 3-h mixed electrode, consistent with its lower interfacial resistance revealed through electrochemical impedance spectroscopy. Overall, the results indicate that dry mixing plays a significant role in the electrochemical performance of the dry-processed NFM cathode. Insufficient or excessive mixing can lead to apparent performance degradation.

As a critical step for dry processing electrodes, mixing determines the component distribution, and it is reasonable to expect that it plays a critical role in the final electrochemical performance [46]. However, such a large change is unexpected. Especially, why the 1-h mixing cathodes cannot cycle is a very intriguing question and has not been reported for the dry processing of any battery electrodes. To understand the underlying mechanism, we then performed additional characterizations on the laminated NFM electrodes prepared by mixing for various durations. No apparent change can be observed from the XRD of the laminated electrode films (Fig. 6(*a*)), suggesting that the hot rolling process for calendaring (at 60 °C) and laminating (at 100 °C) does not affect the bulk structure of the NFM cathodes. The cross-sectional SEM and elemental mappings, on the other hand, show distinct results for the 1-h mixing cathodes. While a more and more uniform distribution of the NFM cathode active material, carbon black, and PTFE can be observed as the mixing duration increases from 3 h to 10 h, the 1-h mixing electrode exhibits the enrichment of PTFE binder on the surface of the electrode (Fig. 6(*b*)). The results indicate that the inhomogeneous distribution of the PTFE

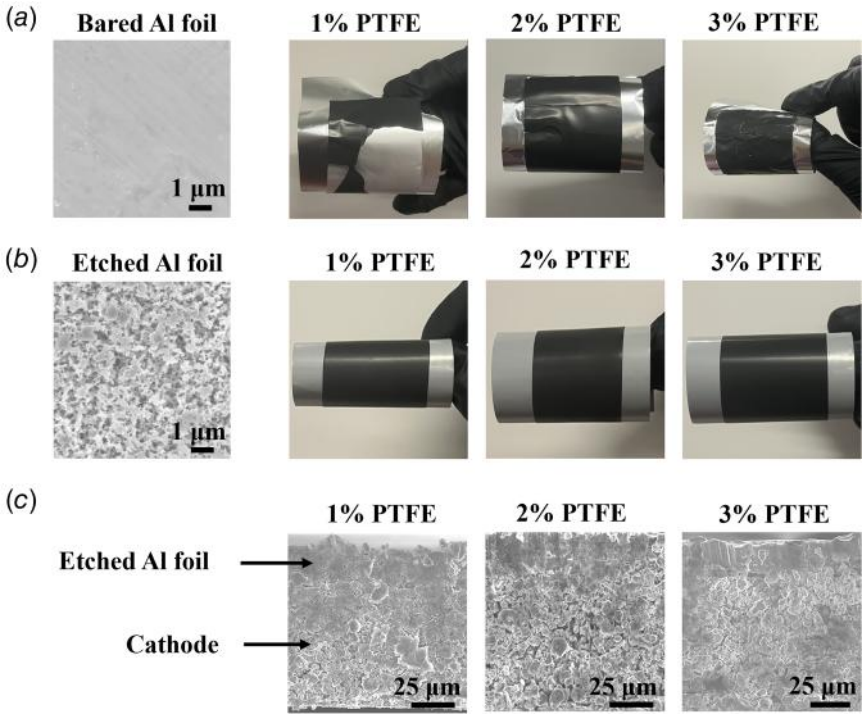

Fig. 3 Laminated electrodes on (*a*) bare Al foil and (*b*) etched Al foil. (*c*) Cross-sectional SEM images of the laminated electrode on etched Al foil. The cathode composite was prepared by mixing for 5 h.

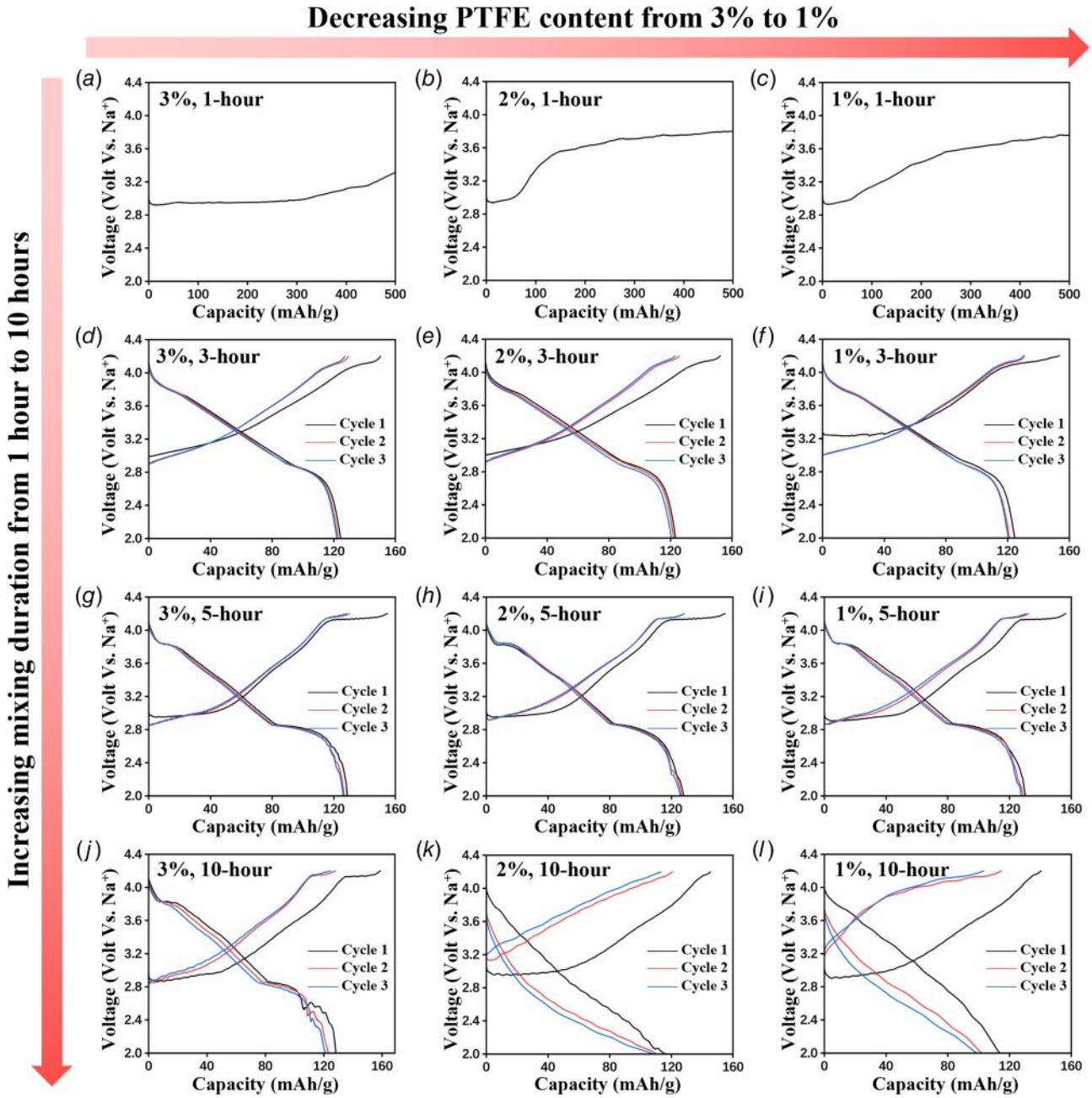

Fig. 4 ((*a*)–(*l*)) Charge/discharge curves of the first three cycles for the laminated NFM cathodes on an etched Al current collector with various PTFE contents and mixing durations. From left to right, the content of PTFE decreases from 3% to 1%. From top to bottom, the mixing duration increases from 1 to 10 h. The electrochemical performances were tested in Na metal half-cells at 0.05C within the voltage range of 2–4.2 V versus Na/Na$^+$.

binder in the cathode due to insufficient mixing can still lead to binder migration to the surface during laminating. It should be noted that PTFE fibrillation can be clearly observed for 3-h and 5-h mixing electrodes, but not much in 1-h and 10-h mixing electrodes (Supplemental Figure 6). Insufficient fibrillation during lower mixing durations can cause agglomerated PTFE clusters, while prolonged mixing can cause shortening or breakage of PTFE fiber bundles, with some fibers becoming trapped within pores or entangled with carbon black [46]. The underlying mechanism for the surface enrichment of PTFE of the dry-processed cathode during laminating is currently unknown. Possible mechanisms include more compression of the surface versus the bulk region during laminating. More careful studies on the microstructure evolution, preferably with the aid of computational tools such as finite element analysis, to understand the effects of PTFE size and distribution on the stress/temperature distribution in the cathode upon lamination would be very helpful. Because PC is a strong polar solvent while PTFE is nonpolar (Supplemental Figure 7), the surface enrichment of PTFE can cause significant wetting issues of the electrolyte with the cathode. The poor wetting availability of PC-based electrolytes on nonpolar separators such as polyolefin-based Celgard separators has been reported [47,48], and in fact, that is why most of the research groups use glass fiber as the separator for SIBs. The nonwetting behavior leads to very limited contact between the liquid electrolyte and the cathode. As a result, only decomposition of the liquid electrolyte will occur during charging, and charging cannot be complete (Fig. 4(*a*)) before all the electrolytes are consumed. As the mixing duration increases to 3 h, a more uniform distribution of PTFE can help mitigate the binder migration (Fig. 6(*b*)), leading

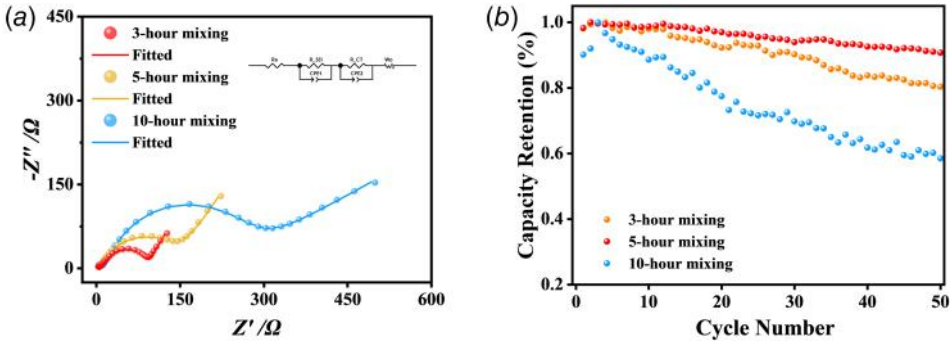

Fig. 5 (*a*) Nyquist plots of dry-processed NFM cathodes with various mixing durations. The electrochemical impedance spectroscopy was measured after the first cycle with a frequency range of 1.5 MHz to 1 Hz. (*b*) Cycling performance of the dry-processed NFM cathodes with various mixing durations. The cycling performance was tested at 1C within the voltage range of 2.0–4.2 V versus Na/Na$^+$.

to effective infiltration of liquid electrolytes into the cathode film. The continuous increase of the mixing duration to 5 h can help to achieve a more uniform distribution of the electrode components in the cathode, leading to improved electrochemical performances.

To understand why extensive mixing for 10 h can deteriorate electrochemical performance, X-ray photoelectron spectroscopy of Ni 2p was used to probe the surface chemistry of the NFM cathode after mixing for various durations (Fig. 7). The binding energies of Ni in the pristine NFM cathode can be attributed to Ni^{2+} (854.5 eV for $2p_{2/3}$ and 871.8 eV for $2p_{1/2}$), Ni^{3+} (856.1 eV for $2p_{2/3}$ and 872.5 eV for $2p_{1/2}$), and a satellite signal at 860.6 and 878.5 eV (Fig. 7(*a*)) [49]. The cathode composite after mixing for 1–5 h (Figs. 7(*b*)–7(*d*)) exhibits similar chemical states. However, extending the mixing duration to 10 h results in the appearance of two distinct minor peaks at 852.3 eV (Ni $2p_{3/2}$) and 869.8 eV (Ni $2p_{1/2}$), characteristic of Ni metal (Ni^0). Although no change in the bulk structure can be observed from the XRD results (Fig. 6(*a*)), extensive milling can lead to a reduction of Ni on the electrode surface. The reduction of transition metals due to ball milling has been reported for lithium layered oxide cathodes [50], and co-milling with carbon black can facilitate the reduction process [51,52]. We believe this is also the reason why the electrochemical performance of the 10-h mixing cathode decreases with the decrease of the binder content (or equivalently, the increase of the content of carbon additive). The surface reduction of Ni can lead to an increase in impedance for Na diffusion, leading to the deterioration of electrochemical performance (Figs. 4 and 5).

The critical role of dry mixing for dry processing NFM cathodes is illustrated in Fig. 8. Insufficient mixing will lead to nonuniform distribution of the cathode active material, carbon black, and PTFE binder. Upon laminating, the PTFE binder can migrate to the electrode surface, leading to wetting issues with the PC-based electrolytes. Increasing the mixing duration helps to achieve uniform distribution of the electrode component, eliminating surface enrichment of PTFE and leading to improved electrochemical performances. However, excessive mixing can also lead to performance degradation due to the reduction of Ni on the surface of the electrode. It should be noted that various mixing approaches, such as tumbler, blender, high-shear, planetary, and mortar mill for batch processing and extrusion/kneading for continuous

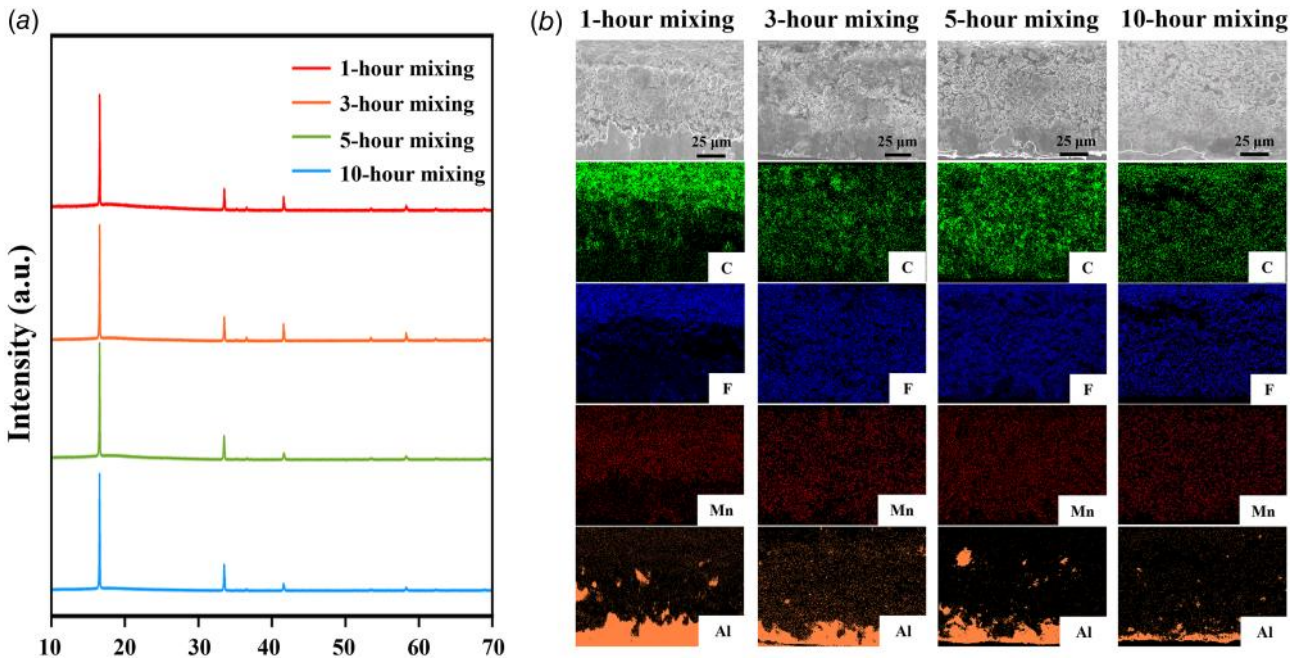

Fig. 6 X-ray diffraction (*a*), cross-sectional SEM and elemental mappings (*b*) of laminated NFM electrodes prepared by mixing for various durations

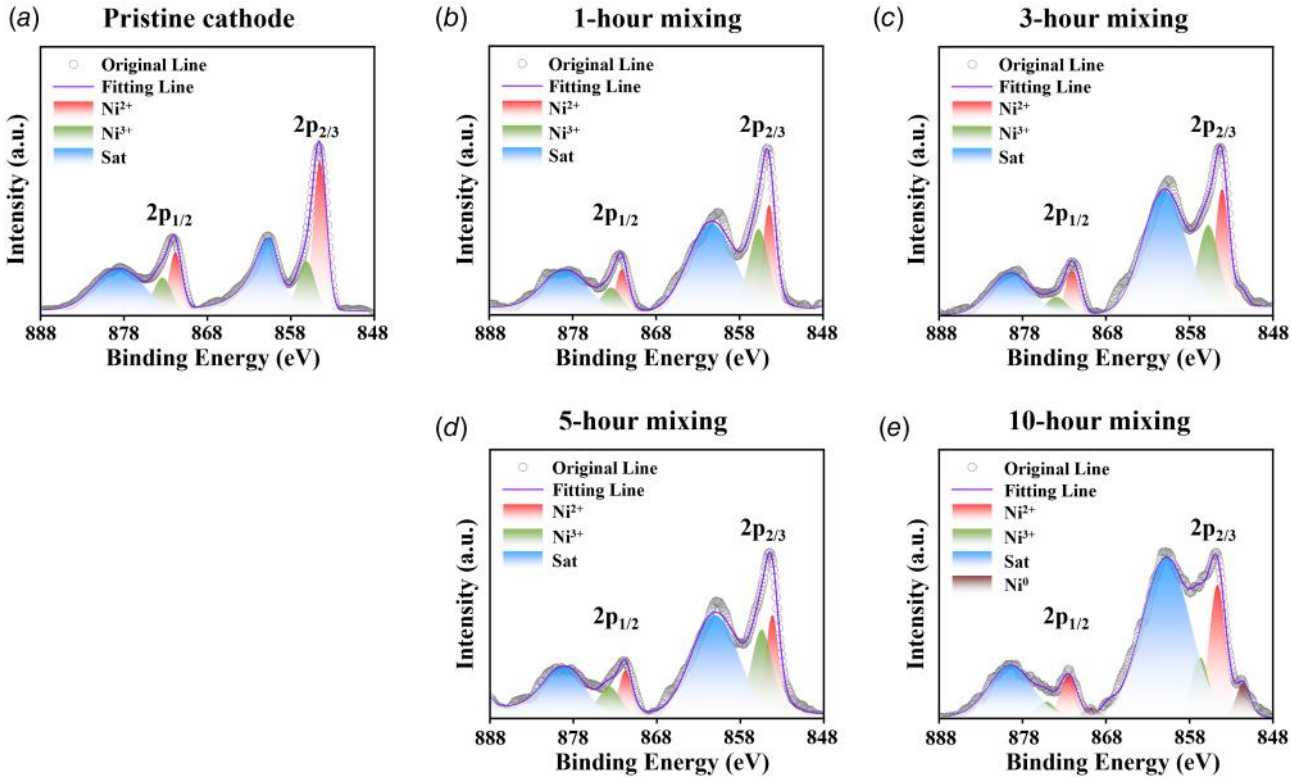

Fig. 7 Ni 2p core level X-ray photoelectron spectra of pristine NFM (*a*) and NFM cathode composite after mixing for various durations ((*b*)–(*e*))

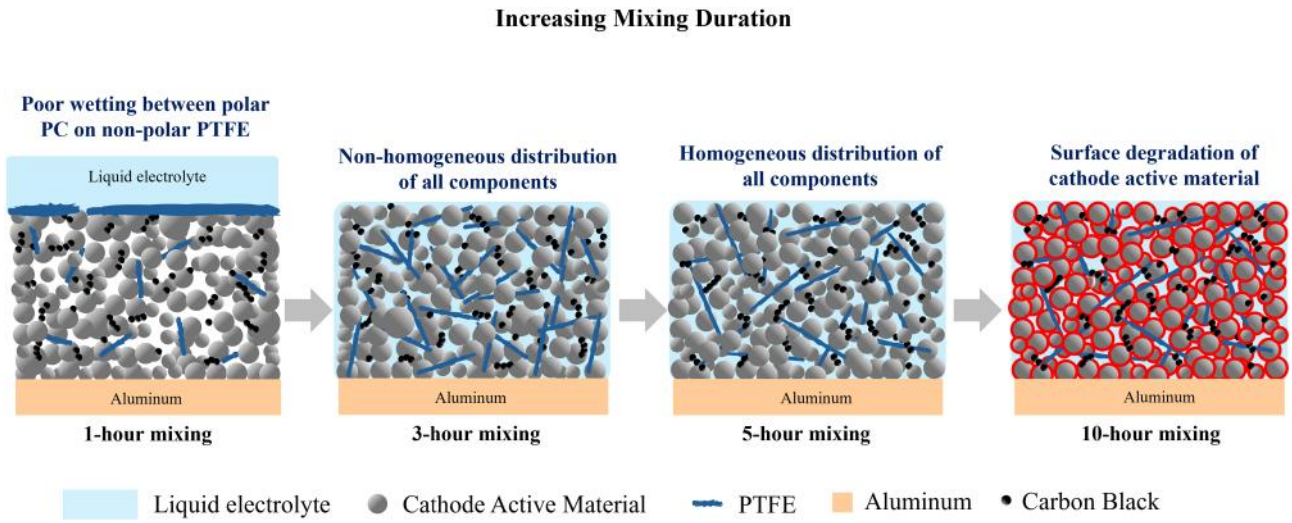

Fig. 8 Effect of mixing duration on binder and carbon distribution in NFM cathode electrode

processing, have their unique advantages and disadvantages [14]. It remains an open question for the community to determine which approach would be optimal. Despite the differences in mixing techniques, the primary mixing mechanisms are essentially diffusion-based, convection-based, shear-based mixing, or a combination of these. We believe that all these mechanisms (diffusion-based, convection-based, and shear-based mixing) exist in the low-rpm planetary ball mill used in the present study. The insights can be transferred to other mixing approaches, especially the continuous extrusion/kneading process, where all three mixing mechanisms coexist. In this regard, we suspect that the underlying principles revealed in this work are transferable to other mixing approaches. Since electrolyte wetting is not a serious concern for LIBs, this work provides novel insights to understand and address processing challenges specific to SIB manufacturing. In addition, the proposed approach also enables us to fabricate an NFM cathode with a thickness of 120 μm and an areal capacity of 4.5 mA h/cm^2 (Supplemental Figure 8), demonstrating the unique advantage of dry processing for preparing thick cathodes.

Conclusion

In summary, we studied the dry processing of O3-type NFM cathode by investigating the effect of binder content, mixing duration, and laminating on various current collectors, on the microstructure and electrochemical performance. We demonstrated that

the PTFE-based approach can be used to fabricate free-standing films for electrodes with various binder contents (from 3 wt% to 1 wt%) and mixed at 100 rpm for various durations (from 1 h to 10 h). Successful lamination of all the free-standing films was also achieved using etched Al foil as the current collector. While all cathodes with various PTFE contents and mixing durations can be successfully laminated on an etched Al current collector, they exhibit drastically different electrochemical performances. The results suggest the predominant role of dry mixing in the performance of dry-processed cathodes. The performance increases as the mixing duration increases from 1 h to 5 h and then decreases with further increasing the duration to 10 h. Surprisingly, we observed that the 1-h mixing electrode cannot be fully charged. SEM analysis of the electrodes suggests the surface enrichment of PTFE for the 1-h mixing electrode, leading to poor wetting of the PC-based liquid electrolyte on the cathode. As a result, only the voltage profile for electrolyte decomposition can be observed. Increasing the mixing durations to 5 h helps achieve uniform binder distribution, which eliminates PTFE surface enrichment and enables the full utilization of the cathode. However, further increasing the mixing durations to 10 h may lead to the reduction of transition metal (Ni) in the NFM cathode, as validated from the XPS analysis, leading to deterioration of the electrochemical performance. The results provide important insights to understand the process–structure–performance for dry electrode manufacturing of sodium-ion batteries.

Acknowledgment

This material is based upon work on the NSF Energy Storage Engine in Upstate New York supported by the National Science Foundation under the NSF Regional Innovation Engines Program (Award No. 2315695).

Conflict of Interest

There are no conflicts of interest.

Data Availability Statement

The datasets generated and supporting the findings of this article are obtainable from the corresponding author upon reasonable request.

References

[1] Li, J., Fleetwood, J., Hawley, W. B., and Kays, W., 2022, "From Materials to Cell: State-of-the-Art and Prospective Technologies for Lithium-Ion Battery Electrode Processing," Chem. Rev., **122**(1), pp. 903–956.
[2] Xiao, J., Cao, X., Gridley, B., Golden, W., Ji, Y., Johnson, S., Lu, D., et al., 2025, "From Mining to Manufacturing: Scientific Challenges and Opportunities Behind Battery Production," Chem. Rev., **125**(13), pp. 6397–6431.
[3] Tao, R., Gu, Y., Du, Z., Lyu, X., and Li, J., 2025, "Advanced Electrode Processing for Lithium-Ion Battery Manufacturing," Nat. Rev. Clean Technol., **1**(2), pp. 116–131.
[4] Kwade, A., Haselrieder, W., Leithoff, R., Modlinger, A., Dietrich, F., and Droeder, K., 2018, "Current Status and Challenges for Automotive Battery Production Technologies," Nat. Energy, **3**(4), pp. 290–300.
[5] Liu, Y., Zhang, R., Wang, J., and Wang, Y., 2021, "Current and Future Lithium-Ion Battery Manufacturing," iScience, **24**(4), p. 102332.
[6] Ludwig, B., Zheng, Z., Shou, W., Wang, Y., and Pan, H., 2016, "Solvent-Free Manufacturing of Electrodes for Lithium-Ion Batteries," Sci. Rep., **6**(1), p. 23150.
[7] Ryu, M., Hong, Y.-K., Lee, S.-Y., and Park, J. H., 2023, "Ultrahigh Loading Dry-Process for Solvent-Free Lithium-Ion Battery Electrode Fabrication," Nat. Commun., **14**(1), p. 1316.
[8] Lu, Y., Zhao, C.-Z., Yuan, H., Hu, J.-K., Huang, J.-Q., and Zhang, Q., 2022, "Dry Electrode Technology, the Rising Star in Solid-State Battery Industrialization," Matter, **5**(3), pp. 876–898.
[9] Zhang, Y., Huld, F., Lu, S., Jektvik, C., Lou, F., and Yu, Z., 2022, "Revisiting Polytetrafluorethylene Binder for Solvent-Free Lithium-Ion Battery Anode Fabrication," Batteries, **8**(6), p. 57.
[10] Kim, N.-Y., Kim, J.-H., Koo, H., Oh, J., Pang, J.-H., Kang, K.-D., Chae, S.-S., Lim, J., Nam, K. W., and Lee, S.-Y., 2024, "Material Challenges Facing Scalable Dry-Processable Battery Electrodes," ACS Energy Lett., **9**(11), pp. 5688–5703.
[11] Bouguern, M. D., Madikere Raghunatha Reddy, A. K., Li, X., Deng, S., Laryea, H., and Zaghib, K., 2024, "Engineering Dry Electrode Manufacturing for Sustainable Lithium-Ion Batteries," Batteries, **10**(1), p. 39.
[12] Zhang, K., Li, D., Wang, X., Gao, J., Shen, H., Zhang, H., Rong, C., and Chen, Z., 2024, "Dry Electrode Processing Technology and Binders," Materials, **17**(10), p. 2349.
[13] Park, J., Kim, J., Kim, J., Kim, M., Song, T., and Paik, U., 2025, "Sustainable and Cost-Effective Electrode Manufacturing for Advanced Lithium Batteries: The Roll-to-Roll Dry Coating Process," Chem. Sci., **16**(16), pp. 6598–6619.
[14] Schumm, B., Dupuy, A., Lux, M., Girsule, C., Dörfler, S., Schmidt, F., Fiedler, M., Rosner, M., Hippauf, F., and Kaskel, S., 2025, "Dry Battery Electrode Technology: From Early Concepts to Industrial Applications," Adv. Energy Mater., **15**(24), p. 2406011.
[15] Duong, H., Shin, J., and Yudi, Y., 2018, "Dry Electrode Coating Technology," Proceedings of the 48th Power Sources Conference, Denver, CO, June 11–13, Vol. 3, pp. 34–37.
[16] Tao, R., Steinhoff, B., Sun, X.-G., Sardo, K., Skelly, B., Meyer, H. M., Sawicki, C., et al., 2023, "High-Throughput and High-Performance Lithium-Ion Batteries Via Dry Processing," Chem. Eng. J., **471**, p. 144300.
[17] Wang, J., Shao, D., Fan, Z., Xu, C., Dou, H., Xu, M., Ding, B., and Zhang, X., 2024, "High-Area-Capacity Cathode by Ultralong Carbon Nanotubes for Secondary Binder-Assisted Dry Coating Technology," ACS Appl. Mater. Interfaces, **16**(20), pp. 26209–26216.
[18] Kwon, K., Kim, J., Han, S., Lee, J., Lee, H., Kwon, J., Lee, J., et al., 2024, "Low-Resistance $LiFePO_4$ Thick Film Electrode Processed With Dry Electrode Technology for High-Energy-Density Lithium-Ion Batteries," Small Sci., **4**(5), p. 2300302.
[19] Kirsch, D. J., Lacey, S. D., Kuang, Y., Pastel, G., Xie, H., Connell, J. W., Lin, Y., and Hu, L., 2019, "Scalable Dry Processing of Binder-Free Lithium-Ion Battery Electrodes Enabled by Holey Graphene," ACS Appl. Energy Mater., **2**(5), pp. 2990–2997.
[20] Zhang, Y., Lu, S., Lou, F., and Yu, Z., 2023, "Solvent-Free Lithium Iron Phosphate Cathode Fabrication With Fibrillation of Polytetrafluoroethylene," Electrochim. Acta, **456**, p. 142469.
[21] Matthews, G. A. B., Wheeler, S., Ramírez-González, J., and Grant, P. S., 2024, "Solvent-Free NMC Electrodes for Li-Ion Batteries: Unravelling the Microstructure and Formation of the PTFE Nano-Fibril Network," Front. Energy Res., **11**, p. 1336344.
[22] Tao, R., Steinhoff, B., Uzun, K., La Riviere, B., Sardo, K., Skelly, B., Hill, R., Cheng, Y.-T., and Li, J., 2023, "Correlation Among Porosity, Mechanical Properties, Morphology, Electronic Conductivity and Electrochemical Kinetics of Dry-Processed Electrodes," J. Power Sources, **581**, p. 233481.
[23] Oh, H., Kim, G.-S., Hwang, B. U., Bang, J., Kim, J., and Jeong, K.-M., 2024, "Development of a Feasible and Scalable Manufacturing Method for PTFE-Based Solvent-Free Lithium-Ion Battery Electrodes," Chem. Eng. J., **491**, p. 151957.
[24] Shin, J., Lee, J. H., Seo, J. K., Ran, W. T. A., Hwang, S. M., and Kim, Y. J., 2022, "Carbon Nanotubes-Coated Ni-Rich Cathodes for the Green Manufacturing Process of Lithium-Ion Batteries," Int. J. Energy Res., **46**(11), pp. 16061–16074.
[25] Sadan, M. K., Lian, G. J., Smith, R. M., and Cumming, D., 2023, "Co, Ni-Free Ultrathick Free-Standing Dry Electrodes for Sustainable Lithium-Ion Batteries," ACS Appl. Energy Mater., **6**(24), pp. 12166–12171.
[26] Yao, W., Chouchane, M., Li, W., Bai, S., Liu, Z., Li, L., Chen, A. X., et al., 2023, "A 5 V-Class Cobalt-Free Battery Cathode With High Loading Enabled by Dry Coating," Energy Environ. Sci., **16**(4), pp. 1620–1630.
[27] Li, G., Xue, R., and Chen, L., 1996, "The Influence of Polytetrafluorethylene Reduction on the Capacity Loss of the Carbon Anode for Lithium Ion Batteries," Solid State Ion., **90**(1–4), pp. 221–225.
[28] Tan, D. H. S., Chen, Y.-T., Yang, H., Bao, W., Sreenarayanan, B., Doux, J.-M., Li, W., et al., 2021, "Carbon-Free High-Loading Silicon Anodes Enabled by Sulfide Solid Electrolytes," Science, **373**(6562), pp. 1494–1499.
[29] Zhou, H., Liu, M., Gao, H., Hou, D., Yu, C., Liu, C., Zhang, D., Wu, J., Yang, J., and Chen, D., 2020, "Dense Integration of Solvent-Free Electrodes for Li-Ion Supercabattery With Boosted Low Temperature Performance," J. Power Sources, **473**, p. 228553.
[30] Hippauf, F., Schumm, B., Dörfler, S., Althues, H., Fujiki, S., Shiratsuchi, T., Tsujimura, T., Aihara, Y., and Kaskel, S., 2019, "Overcoming Binder Limitations of Sheet-Type Solid-State Cathodes Using a Solvent-Free Dry-Film Approach," Energy Storage Mater., **21**, pp. 390–398.
[31] Jiang, T., He, P., Liang, Y., and Fan, L.-Z., 2021, "All-Dry Synthesis of Self-Supporting Thin $Li_{10}GeP_2S_{12}$ Membrane and Interface Engineering for Solid-State Lithium Metal Batteries," Chem. Eng. J., **421**, p. 129965.
[32] Lee, D. J., Jang, J., Lee, J.-P., Wu, J., Chen, Y.-T., Holoubek, J., Yu, K., et al., 2023, "Physio-electrochemically Durable Dry-Processed Solid-State Electrolyte Films for All-Solid-State Batteries," Adv. Funct. Mater., **33**(28), p. 2301341.
[33] Han, S. A., Suh, J. H., Park, M.-S., and Kim, J. H., 2025, "High-Loading Dry-Electrode for All Solid-State Batteries: Nanoarchitectonic Strategies and Emerging Applications," Electrochem. Energy Rev., **8**(1), p. 5.
[34] Hong, J., Yoon, J., Park, J.-W., Ha, Y.-C., Lee, J., and Hwang, I., 2025, "Optimization of PTFE Fibrillation in Dry Electrode Process for Scalable All-Solid-State Battery Manufacturing," J. Power Sources, **655**, p. 237925.
[35] Hu, J.-K., Yuan, H., Yang, S.-J., Lu, Y., Sun, S., Liu, J., Liao, Y.-L., Li, S., Zhao, C.-Z., and Huang, J.-Q., 2022, "Dry Electrode Technology for Scalable and Flexible High-Energy Sulfur Cathodes in All-Solid-State Lithium-Sulfur Batteries," J. Energy Chem., **71**, pp. 612–618.

[36] Usiskin, R., Lu, Y., Popovic, J., Law, M., Balaya, P., Hu, Y.-S., and Maier, J., 2021, "Fundamentals, Status and Promise of Sodium-Based Batteries," Nat. Rev. Mater., **6**(11), pp. 1020–1035.
[37] Yabuuchi, N., Kubota, K., Dahbi, M., and Komaba, S., 2014, "Research Development on Sodium-Ion Batteries," Chem. Rev., **114**(23), pp. 11636–11682.
[38] Abraham, K., 2020, "How Comparable Are Sodium-Ion Batteries to Lithium-Ion Counterparts?," ACS Energy Lett., **5**(11), pp. 3544–3547.
[39] Yao, A., Benson, S. M., and Chueh, W. C., 2025, "Critically Assessing Sodium-Ion Technology Roadmaps and Scenarios for Techno-economic Competitiveness Against Lithium-Ion Batteries," Nat. Energy, **10**(3), pp. 404–416.
[40] Liang, X., Hwang, J.-Y., and Sun, Y.-K., 2023, "Practical Cathodes for Sodium-Ion Batteries: Who Will Take the Crown?," Adv. Energy Mater., **13**(37), p. 2301975.
[41] Li, F., Tang, W., Wu, J., Zhang, L., Mu, A., and Chen, Z., 2024, "Decoding Air-Exposure Degradation Chemistry and Improving Strategy for Layered Sodium Transition Metal Oxide Cathodes," Adv. Energy Mater., **14**(41), p. 2401564.
[42] Qin, N., Jin, L., and Zheng, J. P., 2025, "Sustainable and High-Energy Pre-Sodiation Cathode Using $Na_2C_2O_4$ and Dry-Processing Method for Sodium-Ion Batteries," Energy Proc., **55**.
[43] Kühn, J., Schmidt, F., Seete, P., Boenke, T., Hoffmann, F. S., Dupuy, A., Schumm, B., Abendroth, T., Althues, H., and Kaskel, S., 2025, "Towards Scalable Production of Sodium-Ion Batteries: Solvent-Free Layered-Oxide Cathodes and Aqueous-Processed Hard Carbon Anodes for Cost-Effective Full-Cell Manufacturing," Batteries Supercaps, **8**(5), p. e202400572.
[44] Wu, J., Tang, W., Yang, H., Lee, D. J., Xu, D., Li, F., Qin, J., et al., 2025, "Micron Size $NaCrO_2$ Particles Enable High-Loading Dry-Processed Electrode for Sodium-Ion Batteries," Small, **21**(23), p. e2501504.
[45] Li, M., Qiu, X., Wei, T., and Dai, Z., 2023, "Study of Predominant Dynamics on the O3-Type Layered Transition-Metal Oxide Cathode by Electrochemical Impedance Spectroscopy for Sodium-Ion Batteries," Langmuir, **39**(25), pp. 8865–8878.
[46] Tao, R., Steinhoff, B., Sawicki, C. H., Sharma, J., Sardo, K., Bishtawi, A., Gibbs, T., and Li, J., 2023, "Unraveling the Impact of the Degree of Dry Mixing on Dry-Processed Lithium-Ion Battery Electrodes," J. Power Sources, **580**, p. 233379.
[47] Wostoupal, O. S., Wang, X., Liu, Q., Xu, T., and Zhang, Z., 2025, "Electrolyte Compatible Separator Materials for Sodium-Ion Battery," J. Electrochem. Soc., **172**(6), p. 060515.
[48] Man, C., Jiang, P., Wong, K., Zhao, Y., Tang, C., Fan, M., Lau, W.-M., et al., 2014, "Enhanced Wetting Properties of a Polypropylene Separator for a Lithium-Ion Battery by Hyperthermal Hydrogen Induced Cross-Linking of Poly(Ethylene Oxide)," J. Mater. Chem. A, **2**(30), pp. 11980–11986.
[49] Biesinger, M. C., Payne, B. P., Grosvenor, A. P., Lau, L. W. M., Gerson, A. R., and Smart, R. S. C., 2011, "Resolving Surface Chemical States in XPS Analysis of First Row Transition Metals, Oxides and Hydroxides: Cr, Mn, Fe, Co and Ni," Appl. Surf. Sci., **257**(7), pp. 2717–2730.
[50] Pan, T., Alvarado, J., Zhu, J., Yue, Y., Xin, H. L., Nordlund, D., Lin, F., and Doeff, M. M., 2019, "Structural Degradation of Layered Cathode Materials in Lithium-Ion Batteries Induced by Ball Milling," J. Electrochem. Soc., **166**(10), pp. A1964–A1971.
[51] Yang, H., and McCormick, P., 1998, "Mechanically Activated Reduction of Nickel Oxide With Graphite," Metall. Mater. Trans. B, **29**(2), pp. 449–455.
[52] Bakhshandeh, S., Setoudeh, N., Ali Askari Zamani, M., and Mohassel, A., 2018, "Carbothermic Reduction of Mechanically Activated NiO–Carbon Mixture: Non-isothermal Kinetics," J. Mining Metall. Sect. B: Metall., **54**(3), pp. 313–322.